Soft Matter

Elasticity of colloidal gels: structural heterogeneity, floppy modes, and rigidity

Journal:	*Soft Matter*
Manuscript ID	SM-COM-01-2020-000053.R1
Article Type:	Communication
Date Submitted by the Author:	21-May-2021
Complete List of Authors:	Rocklin, D.; Georgia Institute of Technology, School of Physics Hsiao, Lilian; North Carolina State University, Chemical and Biomolecular Engineering Szakasits, Megan; University of Michigan, Chemical Engineering Solomon, Michael; University of Michigan, Chemical Engineering Mao, Xiaoming; University of Michigan, Physics

Soft Matter

ARTICLE TYPE

Cite this: DOI: 00.0000/xxxxxxxxxx

Elasticity of colloidal gels: structural heterogeneity, floppy modes, and rigidity†

D. Zeb Rocklin,*[a,b] Lilian Hsiao,[c] Megan Szakasits,[d] Michael J. Solomon[d] and Xiaoming Mao*[a]

Received Date
Accepted Date

DOI: 00.0000/xxxxxxxxxx

Rheological measurements of model colloidal gels reveal that large variations in the shear moduli as colloidal volume-fraction changes are not reflected by simple structural parameters such as the coordination number, which remains almost a constant. We resolve this apparent contradiction by conducting a normal-mode analysis of experimentally measured bond networks of gels of colloidal particles with short-ranged attraction. We find that structural heterogeneity of the gels, which leads to floppy modes and a nonaffine-affine crossover as frequency increases, evolves as a function of the volume fraction and is key to understanding the frequency-dependent elasticity. Without any free parameters, we achieve good qualitative agreement with the measured mechanical response. Furthermore, we achieve universal collapse of the shear moduli through a phenomenological spring-dashpot model that accounts for the interplay between fluid viscosity, particle dissipation, and contributions from the affine and non-affine network deformation.

1 Introduction

Colloidal gels are soft matter with disordered structure and slow dynamics due to short-range, attractive inter-particle forces[1,2]. The attractive interactions stabilize a sample-spanning network of particles. This network displays mechanical features of a soft solid, including a finite linear elastic modulus at low frequency, the existence of a yield stress at the low shear rate limit[3,4], and time-dependent thixotropic properties[5,6]. Recent work has established how pair potential interactions and colloidal volume fraction determine the onset of gelation[7–16]. Observation, by simulation and experiment, of the coincidence of this gel line and the spinodal decomposition boundary suggests a mechanism in which phase instability generates connected regions of high colloidal density. A prevailing hypothesis is that if the colloidal density of these regions is greater than the glass transition volume fraction, gelation can occur through this heterogeneous mechanism of sequential phase separation and vitrification[14,17,18]. Alternatively, attractive interactions of sufficient strength might yield gelation through a homogeneous mechanism in which low-coordination number (i.e., the number of a particle's contacting neighbors) networks are stabilized, perhaps only kinetically, through a mechanism such as dynamic percolation[19,20]. Functionally, either gelation mechanism yields a structure in which nearly all particles are spatially localized within a single, sample-spanning network.

This paper addresses the outstanding fundamental question of how such a low volume fraction, disordered network of the colloid mediates the solid-like rheological properties that are characteristic of gels.

The low-frequency elasticity of colloidal gels has been predicted from pair potential interactions and microstructure in a few instances. The linear elastic modulus of fractal cluster gels has been modeled by a microrheological approach, in which the elastic modulus is inversely proportional to the fractal cluster radius and the mean-squared localization length of colloids in the gel. The localization length can be predicted by summing over the hierarchy of normal modes of the fractal cluster[21]. Mode coupling theory has also been applied to yield the elastic modulus from the localization length in attractive colloidal systems[22], albeit with a rescaling required for the effects of voids and clusters in the gel[15,23–25]. A key feature of these theories for the linear elastic modulus is that they connect linear elasticity through two ensemble-averaged quantities, a dynamical localization length and a structural (cluster or particle) scale. The structural heterogeneity of colloidal gels, which originates from dynamical arrest and phase separation and plays an important role in the elasticity of gels[26], is therefore captured in these models

[a] Department of Physics, University of Michigan, 450 Church St., Ann Arbor, Michigan, 48109, Email: maox@umich.edu
[b] School of Physics, Georgia Institute of Technology, 837 State Street, Atlanta, Georgia, 30332, Email: zebrocklin@gatech.edu
[c] Department of Chemical and Biomolecular Engineering, North Carolina State University, 911 Partners Way, Raleigh, North Carolina 27606
[d] Department of Chemical Engineering, University of Michigan, 2300 Hayward St., Ann Arbor, Michigan, 48109

† Electronic Supplementary Information (ESI) available: [details of any supplementary information available should be included here]. See DOI: 10.1039/cXsm00000x/

in only a mean-field way. Moreover, frequency-dependent properties, which would require incorporation of viscous losses, have not been accounted for in these studies.

Here we address these gaps by presenting a theoretical framework to not only compute the frequency-dependent linear viscoelastic modulus of colloidal gels, but also reveal the physics behind the frequency, volume-fraction, and attraction strength dependence of the modulus, as a result of the interplay between floppy modes and mechanical stability, and between affine and nonaffine deformations. Our theory includes two parallel approaches to characterize the elasticity of colloidal gels. The first approach is a microscopic model, in which we take particle positions from measured 3D microstructures of a model colloidal gel and perform normal mode analysis. Harmonic springs are introduced between neighboring particles with a spring constant extracted from the inter-particle potential in the presence of thermal fluctuations; viscous drag against the affinely-deforming fluid medium is also included in the model. This microscopic model predicts frequency-dependent shear moduli, showing a crossover from low frequency nonaffine deformations with low rigidity to high frequency affine deformation with high rigidity, in good qualitative agreement with our rheological measurements. The origin of this crossover is a collection of floppy modes, i.e., particle displacements that don't change bond lengths[27–33], which are present in colloidal gels as a result of their low coordination numbers and structural heterogeneities. This observation leads to our second approach, a phenomenological spring-dashpot model based on the Maxwell–Wiechert model of linear solids[34,35], incorporating affine and nonaffine limits of deformations and the viscous drag. We obtain good collapse of our experimental shear modulus using this phenomenological model. Compared to the first approach, this phenomenological model needs no information about the microstructures. The collapse supports the nonaffine-affine crossover scenario for the frequency dependent shear modulus at different attraction strength and volume fractions.

Another important factor that affects gel rheology is hydrodynamic interactions, which has been shown to significantly lower the critical volume fraction for gelation[36,37]. Recently, in a comprehensive study that combined experiments and simulations[38], it was shown that gel linear viscoelasticity at higher volume fractions can still be well described with Brownian Dynamics[5,6,39,40] when entropic and hydrodynamic interactions contributions are captured via rescaling. Here we take this simple approach, since the focus of this paper are the structure and rigidity aspects of colloidal gel rheology.

2 Experiment

The 3D structure of the colloidal gels is studied in conjunction with linear rheological characterization. We synthesize poly(methyl methacrylate) (PMMA) colloids (radius $a = 0.58\mu m \pm$ 4% characterized with scanning electron microscopy) that are sterically stabilized and suspended at various volume fractions ($\phi = 0.15, 0.20, 0.25, 0.30, 0.35,$ and 0.40) with charge screening. Non-adsorbing polystyrene (radius of gyration $R_g = 41$ nm, $\approx \%7$ of colloidal radius, in accord with previous experiments[41–45]) is added at a dilute concentration ($c/c^* = 0.4$ and 0.5, where c^* is the overlap concentration of the depleting polymer) to induce a short-ranged depletion attraction ($\xi = R_g/a = 0.07$) that leads to gelation.

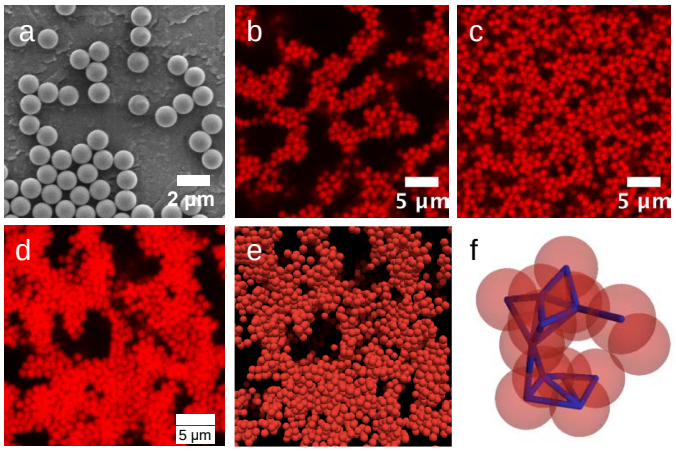

Fig. 1 (a) Scanning electron micrographs of sterically stabilized PMMA colloids used to generate gel networks. Representative confocal laser scanning microscopy (CLSM) images of colloidal gels at (b) $\phi = 0.15, c/c^* = 0.4$ and (c) $\phi = 0.40, c/c^* = 0.4$. We collect raw images in 3D and use image processing to detect particle centroids for theoretical modeling. (d) is a 3D stack of a gel ($\phi = 0.15, c/c^* = 0.4$) that has been projected onto a 2D plane; (e) shows a rendering of the microstructure after image analysis. (f) Bonds of attractive contact (blue) between particles (red) are constructed for particle pairs of distance below $1.5\mu m$.

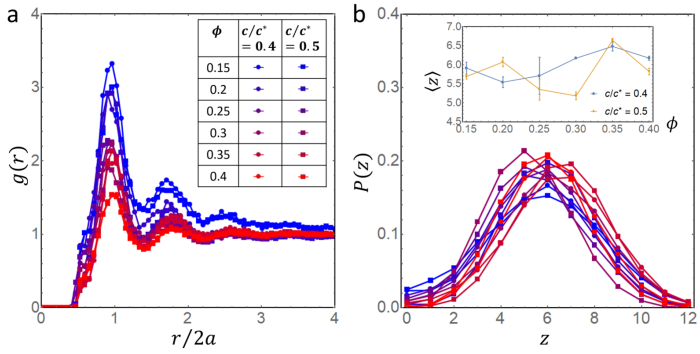

Fig. 2 (a) Pair correlation function $g(r)$ for each ϕ and c/c^*. (b) distribution of coordination number, $P(z)$. Inset shows the mean, $\langle z \rangle$ as a function of ϕ at $c/c^* = 0.4, 0.5$.

Gels are allowed to quiescently equilibrate for 30 minutes prior to imaging and rheological characterization [more details in the Electronic Supplementary Information (ESI)]. Figure 1 shows that as ϕ increases, the void space of the heterogeneous microstructure is replaced with colloid-rich networks with densely packed, high coordination number regions. The confocal microscopy images are obtained from three independent locations within the same sample, at a distance of $\geq 15\mu$m above the coverslip. In order to locate particle centroids, we identify the particles using a local regional maximum of intensity in 3D space after smoothing out digital noise in the images[46]. Fig. 1(e) is a

rendering of the 3D microstructure in Fig. 1(c), which shows that the 3D structural information used as inputs in our microscopic theory are representative of the gel structure captured from the experiments.

The radial distribution function, $g(r)$, and the coordination number distribution, $P(z)$, are directly computed using the location of the particles in 3D. The $g(r)$ for gels with $c/c^* = 0.4$ and $c/c^* = 0.5$ are plotted in Fig. 2(a). Particles are considered to be in attractive contact if their separation distance is less that that of the first minimum in the $g(r)$, which is $1.5\mu m$. A sensitivity analysis (SI) reveals that the response is qualitatively robust for cutoffs ranging from this choice to the naive theoretical cutoff, $2(a+R_g) = 1.24\mu m$. Figure 2(b) and inset show that the mean coordination number, $\langle z \rangle$, remains close to six despite the changes in c/c^* and ϕ. The quantitatively similar nature of the structure for gels with $0.15 \leq \phi \leq 0.40$ is surprising in light of rheological measurements (Fig. 3), in which the low-frequency shear modulus spans more than two orders of magnitude as a function of volume fraction. As we discuss below, the large variation of shear modulus results from the evolution of the structural heterogeneity, which changes the normal mode structures of the gel, whose coupling with macroscopic deformations determines the elastic moduli.

3 Microscopic Model

We model colloidal gels as disordered spring networks. Particle positions are taken from 3D confocal images of the gels, and springs are added to pairs of particles in contact with one another. Additionally, we treat the fluid medium as moving affinely (i.e., homogeneous deformation field) in response to the external stress, allowing us to approximate the complex effects of the hydrodynamics[36,37,47,48] as a simple Stokes drag against this affine background[49–51]. The resulting force on particle i is:

$$\mathbf{F}_i = -k_{\text{eff}} \sum_{\langle i,j \rangle} \hat{\mathbf{r}}_{ij} \left[\hat{\mathbf{r}}_{ij} \cdot \left(\mathbf{u}_i - \mathbf{u}_j \right) \right] + 6\pi i \omega \eta_f a \left(\mathbf{u}_i - \mathbf{u}_i^{\text{aff}} \right), \qquad (1)$$

where $\hat{\mathbf{r}}_{ij}$ is the unit vector pointing from particle i to its bonded neighbor j, $\mathbf{u}_i$ is the displacement of particle i from its equilibrium position, $\mathbf{u}_i^{\text{aff}}$ is the affine displacement which is $(\Lambda - I) \cdot \mathbf{r}_i$ for a particle with equilibrium position $\mathbf{r}_i$ under deformation gradient Λ, $\eta_f = 0.0025\,\text{Pa}\cdot\text{s}$ is the fluid viscosity, ω is the frequency of the driving force (with the physical portion of quantities scaled by $\exp(i\omega t)$ being the real part), and k_{eff} the effective spring constant.

In order to obtain this spring constant, we start from the Asakura-Oosawa potential for depletion interaction $U_{\text{AO}}(r)$, where r is the distance between the centers of the two particles[52]. Additionally, the particles also experience a screened electrostatic repulsion of the DLVO form, $U_{\text{DLVO}}(r)$, leading to a total potential $U(r)$[53,54]. Expressions for these potentials are included in the SI. While this interaction is not harmonic, given that the depth of this potential is $\approx 5.7\,k_BT$ ($c/c^* = 0.4$) and $\approx 7.9\,k_BT$ ($c/c^* = 0.5$), thermal fluctuations cause the distance between the pair of particles to explore a significant portion of this potential well. Thus, instead of taking the curvature of $U(r)$ at the minimum, the effective spring constant should be extracted from the thermal fluctuations of the pair distance through a fluctuation-dissipation approach as described in the SI, resulting in an effective spring constant that accommodates the nonlinearity of the pair interaction over thermal fluctuations in the pair separations:

$$k_{\text{eff}} = \frac{k_BT}{\langle r^2 \rangle - \langle r \rangle^2}, \qquad (2)$$

where $\langle r^2 \rangle, \langle r \rangle^2$ are evaluated over all possible bonded separation lengths, $2a \leq r \leq 2\left(a + R_g\right)$ for an isolated pair with Boltzmann factor $e^{-U(r)/k_BT}$. This results in spring constants of 9.2×10^{-5} N/m and 1.8×10^{-4} N/m for depletant concentrations c/c^* of 0.4 and 0.5, respectively. In Fig. 3(a), we compare the potentials, with the horizontal and vertical offset of the harmonic effective potential chosen to be the average separation $\langle r \rangle$ and the average energy under thermal fluctuations (note that only the curvature of the potential, k_{eff}, enters our calculation for shear modulus below). A similar calculation was used to estimate the effective spring constant of weakly-aggregated colloidal gels[13].

This model permits the direct calculation of the mode structure of the several thousand particles in the CLSM scan (Fig. 3b). We find that in all samples the calculation indicates a significant fraction of collective modes (on the order 10%) are floppy modes, as a result of the low coordination numbers and the heterogeneous structures[27,28]. It is worth noting that the existence of these floppy modes does not preclude a finite shear modulus, as the macroscopic shear deformation may not completely overlap with these floppy modes, most of which are localized. The rest of the vibrational modes exhibit a plateau in the density of states (DOS), sharing similarity to the DOS in jammed packings[55].

This spring network model recovers the rheological storage shear moduli G' without any free parameters, as shown in Fig. 3(c-d) (agreement for the loss shear moduli G'' is included in the SI). To determine the model's storage modulus $G'(\omega)$, we subject boundary particles to oscillating shear displacements, allow internal dynamics given by Eq. (1) and measure the boundary force, as described in more detail in the SI. We find three regimes of behavior. In the high-frequency regime, beyond $\sim 10^4$ rad/s, Stokes forces dominate, driving the gel to affine displacements and resulting in a plateau in the storage modulus. In the low-frequency regime, in contrast, the drag term is negligible and the system is free to assume nonaffine deformations (i.e., a spatially varying strain field due to heterogeneity[56]), dominated by the floppy modes, to minimize energy while accommodating the shear boundary conditions. For most samples, these boundary conditions cannot be met purely with the floppy modes, resulting in a low-frequency plateau, in accord with previous studies that observed finite elastic moduli even below the isostatic point[26]. The upper limit frequency of this regime is where the fluid drag is comparable to the nonaffine shear modulus, as we discuss more below. In the third regime, which corresponds to intermediate frequencies, shear moduli increase somewhat sublinearly in frequency, displaying nontrivial behavior as nonaffinity is reduced. This is the regime accessible via the rheometer, and good qualitative agreement is found between direct measurements and the spring model developed from the scans as shown in Fig. 3. The

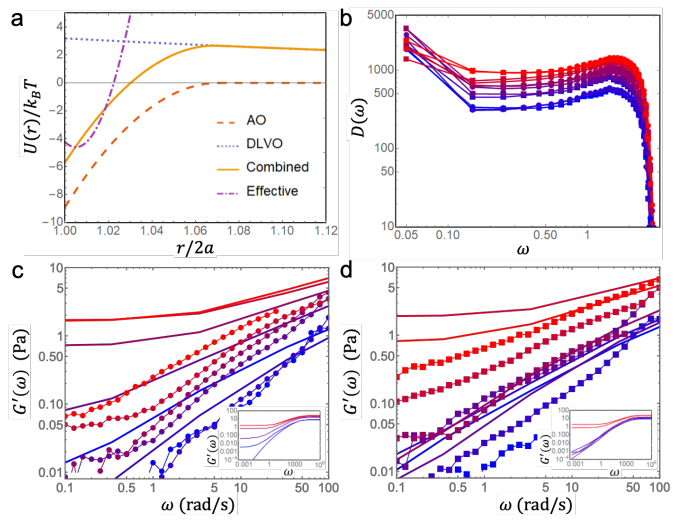

Fig. 3 (a) Interaction potential between a pair of particles and the harmonic effective potential with spring constant $k_{\rm eff}$ as in Eq. (2). (b) Vibrational density of states calculated from microstructures. Floppy modes (modes with $\omega = 0$) are included in the peak at $\omega = 0.05$ (frequency normalization $\sqrt{k_{\rm eff}/m}$ where m is particle mass), which gives the number of modes in the system within $0 \le \omega < 0.1$. (c-d) Experimental (symbols) and model (curves, same color of symbol and curve correspond to the same parameters) values of $G'(\omega)$ at $c/c^* = 0.4$ (c) and $c/c^* = 0.5$ (d) for different values of ϕ. The symbols and colors in (b-d) are the same as in Fig. 2. Insets show the same plot of model result G' in a wider frequency window, illustrating the crossover.

.

model (without free parameters) accurately captures the range of moduli observed, the sublinear power-law dependence on frequency and the rough dependence on concentrations of particles and depletant, but falls short of reliable quantitative agreement. The discrepancies at low frequencies between microscopic model and experimental data, especially for high density samples, are due to the fact that the microscopic models are based on microstructures in a small scan window. The true shear response from rheological measurements at the lowest frequencies involves significantly nonaffine deformations over volumes large compared to the scan window. Similar types of nonaffine-affine crossovers have been discussed theoretically in the context of disordered spring networks near isostaticity[50,51].

4 Phenomenological Spring-Dashpot Model

The agreement between our microscopic model and the rheological data suggests a phenomenological picture as shown in Fig. 4(a-b). The shear response of the gel is a combination of the following effects: at zero frequency shear deformations of the gel are determined by energy minimization which projects the deformation to a collection of the lowest frequency modes, yielding the nonaffine shear modulus $G_{\rm NA}$ (which may vanish at small ϕ). We characterize this shear modulus component by a spring of spring constant $G_{\rm NA}$ in our diagram. At high frequencies, the fluid which moves affinely drags particles in the gel to move affinely as well, resulting in a much higher shear modulus $G_{\rm A}$. This increase of shear modulus $G_{\rm A} - G_{\rm NA}$ is a result of fluid drag, so it can be characterized by a spring of spring constant $G_{\rm A} - G_{\rm NA} \simeq G_{\rm A}$ in series with the fluid drag which is characterized by a viscous dashpot of viscosity η_c (where the subscript c denote for coupling between fluid and particles). In addition, in parallel with parts of the diagram described above, there is also the fluid contribution with viscosity η_f. Because our systems are driven below the yield stress, we do not include a sliding block of the sort that is sometimes incorporated to permit yielding.

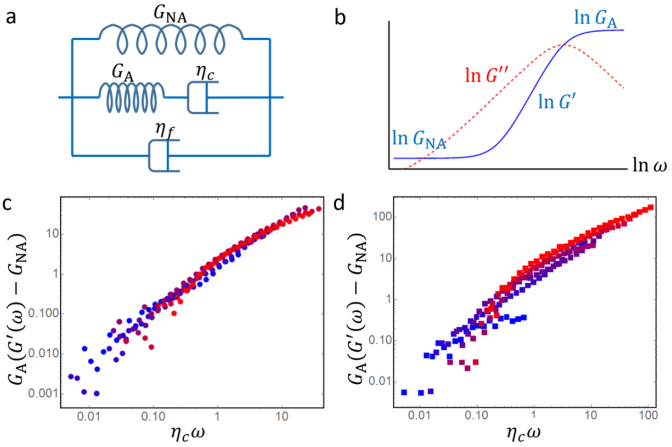

Fig. 4 (a) Diagram for the phenomenological spring-dashpot model. (b) Schematic shear modulus - frequency relation for the model in (a). (c-d) Collapse of $G'(\omega)$ data using the formula in Eq. (4) for $c/c^* = 0.4$ (c) and $c/c^* = 0.5$ (d). Colors and symbols are the same as in Fig. 2.

Adding up these contributions, the total shear modulus is

$$G(\omega) = G_{\rm NA} + \left[G_{\rm A}^{-1} - (i\eta_c\omega)^{-1}\right]^{-1} - i\eta_f\omega. \qquad (3)$$

Taking the real and imaginary parts of this equation and assuming that $\eta_c\omega \ll G_{\rm A}$, we have

$$G_{\rm A}[G'(\omega) - G_{\rm NA}] = (\eta_c\omega)^2$$

$$G''(\omega) = (\eta_c + \eta_f)\omega, \qquad (4)$$

which suggests that our rheological data $G'(\omega)$ can be collapsed into a master straight line.

To obtain this collapse, we use $G_{\rm A}$ from a simple estimate that all bonds are in random orientations (uniformly, independently distributed) in the network (see ESI for derivation),

$$G_{\rm A} \simeq \frac{\phi\langle z\rangle k_{eff}}{10\pi a}. \qquad (5)$$

The same formula for gel affine shear modulus has been discussed in Refs.[57,58]. We obtain $G_{\rm NA}$ from the low-frequency plateau in $G'(\omega)$ data (computed as average $G'(\omega)$ for $\omega < 0.2$ rad/s). We extract η_c for each set of parameters $(\phi, c/c^*)$ by fitting $G''(\omega) - \eta_f\omega$ as a linear function of ω for $\omega < 1$ rad/s (where the linear approximation works well) according to Eq. (4). It is worth noting that although the affine shear modulus $G_{\rm A}$ is linear in ϕ, the nonaffine one $G_{\rm NA}$ increases much faster than linearly (see the SI for a list of fitting parameters). Using these parameters, we obtain good collapse of $G'(\omega)$ according to Eq. (4) into a straight line in the log-log plot, as shown in Fig. 4c-d. Interestingly, the slope

of the line, instead of 2, is closer to 1, indicating perhaps more complicated couplings between the heterogeneous gel structure with the fluid than a simple dashpot. Related types of scaling collapse of $G(\omega)$, but focusing on the low-frequency plateau to intermediate-frequency regime crossover which yields a nonlinear master curve, have been discussed in Refs.[7,59]. In contrast with previous work, we include the high-frequency plateau and explain the origin of the parameters from the network mechanics and derive them independently rather than fitting from the collapse.

This collapse supports the nonaffine-affine crossover scenario for the frequency dependent shear modulus of colloidal gels, and provides a simple formula to predict gel rheology. This crossover also shares interesting similarities with the rheology of arrested phase separation in protein suspensions[60], although both plateaus of G' at high and low frequencies in Ref.[60] increase exponentially with ϕ, indicating more complicated interactions between the network and the fluid.

5 Conclusions

We propose a theoretical framework to understand mechanical properties of colloidal gels, including a method to compute the frequency-dependent linear shear modulus $G'(\omega)$ from experimentally observed microstructures, and a phenomenological spring-dashpot model that collapses $G'(\omega)$ into a master line for different ϕ and c/c^*. Our theory is based on analyzing normal modes of the colloidal gel structure as a spring network, which exhibits a large number of floppy modes due to the structural heterogeneity, and gives rise to dramatically different static shear moduli at different ϕ and c/c^*. The static shear modulus, which involves nonaffine deformations of the network, gives way to a much higher affine shear modulus as a result of viscous drag of the fluid as frequency increases. The affine shear modulus displays a much smaller spread as a function of ϕ and c/c^*, because it is not sensitive to the structural heterogeneity. Our computational model, without any free parameters, accurately predicts the range of moduli observed, roughly how they vary between samples of different particle and depletant densities, and their sub-linear dependence on frequency.

Detailed characterization of the heterogeneous network structure, especially at larger scales which is important in understanding the low frequency shear modulus, and how that affects the gelation transition, as well as how we can control the heterogeneity in experiment and thus tune mechanical response of gels, may be interesting questions in future studies[61,62].

Conflicts of interest

There are no conflicts to declare.

Acknowledgements

Acknowledgment – We acknowledge support from NSF under grant number DMR-1609051 (XM), CBET-1232937 (LCH and MJS), and ICAM and Bethe/KIC postdoctoral fellowships (DZR).

Notes and references

1 E. Zaccarelli, *Journal of Physics: Condensed Matter*, 2007, **19**, 323101.
2 V. Trappe and P. Sandkuhler, *Curr. Opin. Colloid Interface Sci.*, 2004, **8**, 494–500.
3 D. Bonn and M. M. Denn, *Science*, 2009, **324**, year.
4 J. Mewis and N. J. Wagner, *Colloidal Suspension Rheology*, Cambridge University Press, 2012.
5 R. G. Larson and Y. Wei, *Journal of Rheology*, 2019, **63**, 477–501.
6 S. Jamali, R. C. Armstrong and G. H. McKinley, *Physical review letters*, 2019, **123**, 248003.
7 V. Trappe and D. A. Weitz, *Phys. Rev. Lett.*, 2000, **85**, 449–452.
8 P. N. Segrè, V. Prasad, A. B. Schofield and D. A. Weitz, *Phys. Rev. Lett.*, 2001, **86**, 6042–6045.
9 A. D. Dinsmore and D. A. Weitz, *Journal of Physics: Condensed Matter*, 2002, **14**, 7581.
10 A. M. Puertas, M. Fuchs and M. E. Cates, *J. Chem. Phys.*, 2004, **121**, 2813–2822.
11 F. Sciortino, S. V. Buldyrev, C. De Michele, G. Foffi, N. Ghofraniha, E. La Nave, A. Moreno, S. Mossa, I. Saika-Voivod, P. Tartaglia and E. Zaccarelli, *Computer physics communications*, 2005, **169**, 166–171.
12 E. Del Gado and W. Kob, *Europhysics Letters*, 2005, **72**, 1032.
13 A. D. Dinsmore, V. Prasad, I. Y. Wong and D. A. Weitz, *Phys. Rev. Lett.*, 2006, **96**, 185502.
14 P. J. Lu, E. Zaccarelli, F. Ciulla, A. B. Schofield, F. Sciortino and D. A. Weitz, *Nature*, 2008, **453**, 499–U4.
15 A. Zaccone, H. Wu and E. Del Gado, *Phys. Rev. Lett.*, 2009, **103**, 208301.
16 J. Colombo and E. Del Gado, *Soft Matter*, 2014, **10**, 4003–4015.
17 G. Foffi, C. De Michele, F. Sciortino and P. Tartaglia, *Journal of Chemical Physics*, 2005, **122**, 224903.
18 C. P. Royall, S. R. Williams, T. Ohtsuka and H. Tanaka, *Nature Materials*, 2008, **7**, 556.
19 C. J. Dibble, M. Kogan and M. J. Solomon, *Physical Review E*, 2006, **74**, 41403.
20 *Langmuir*, 2012, **28**, 1866–1878.
21 A. H. Krall and D. A. Weitz, *Phys. Rev. Lett.*, 1998, **80**, year.
22 Y.-L. Chen and K. S. Schweizer, *The Journal of chemical physics*, 2004, **120**, 7212–7222.
23 S. Ramakrishnan, Y.-L. Chen, K. S. Schweizer and C. F. Zukoski, *Phys Rev E*, 2004, **70**, 40401.
24 K. Kroy, M. Cates and W. Poon, *Physical review letters*, 2004, **92**, 148302.
25 L. C. Hsiao, H. Kang, K. H. Ahn and M. J. Solomon, *Soft Matter*, 2014, **10**, 9254–9259.
26 L. C. Hsiao, R. S. Newman, S. C. Glotzer and M. J. Solomon, *Proceedings of the National Academy of Sciences*, 2012, **109**, 16029–16034.
27 D. J. Jacobs and M. F. Thorpe, *Phys. Rev. Lett.*, 1995, **75**, 4051–4054.
28 T. Lubensky, C. Kane, X. Mao, A. Souslov and K. Sun, *Reports on Progress in Physics*, 2015, **78**, 073901.

29 X. Mao, N. Xu and T. C. Lubensky, *Phys. Rev. Lett.*, 2010, **104**, 085504.

30 W. G. Ellenbroek and X. Mao, *Europhys. Lett.*, 2011, **96**, year.

31 L. Zhang, D. Z. Rocklin, B. G.-g. Chen and X. Mao, *Phys. Rev. E*, 2015, **91**, 032124.

32 X. Mao, A. Souslov, C. I. Mendoza and T. C. Lubensky, *Nature Communications*, 2015, **6**, 5968.

33 X. Mao and T. C. Lubensky, *Annual Review of Condensed Matter Physics*, 2018, **9**, 413–433.

34 E. Wiechert, *PhD thesis*, 1889.

35 D. Gutierrez-Lemini, *Engineering viscoelasticity*, Springer, 2016.

36 A. Furukawa and H. Tanaka, *Physical Review Letters*, 2010, **104**, 245702.

37 Z. Varga, G. Wang and J. Swan, *Soft Matter*, 2015, **11**, 9009–9019.

38 L. C. Johnson, R. N. Zia, E. Moghimi and G. Petekidis, *Journal of Rheology*, 2019, **63**, 583–608.

39 G. J. Donley, J. R. de Bruyn, G. H. McKinley and S. A. Rogers, *Journal of Non-Newtonian Fluid Mechanics*, 2019, **264**, 117–134.

40 R. Larson, *Journal of Rheology*, 2015, **59**, 595–611.

41 A. Boromand, S. Jamali and J. M. Maia, *Soft matter*, 2017, **13**, 458–473.

42 N. Park and J. C. Conrad, *Soft matter*, 2017, **13**, 2781–2792.

43 E. Moghimi, A. R. Jacob, N. Koumakis and G. Petekidis, *Soft Matter*, 2017, **13**, 2371–2383.

44 K. A. Whitaker, Z. Varga, L. C. Hsiao, M. J. Solomon, J. W. Swan and E. M. Furst, *Nature communications*, 2019, **10**, 1–8.

45 S. Jamali, R. C. Armstrong and G. H. McKinley, *Materials Today Advances*, 2020, **5**, 100026.

46 J. C. Crocker and D. G. Grier, *Journal of colloid and interface science*, 1996, **179**, 298–310.

47 P. Hoogerbrugge and J. Koelman, *Europhysics Letters*, 1992, **19**, 155.

48 J. Vermant and M. Solomon, *Journal of Physics: Condensed Matter*, 2005, **17**, R187.

49 D. J. Durian, *Phys. Rev. Lett.*, 1995, **75**, 4780–4783.

50 B. P. Tighe, *Physical review letters*, 2012, **109**, 168303.

51 M. Yucht, M. Sheinman and C. Broedersz, *Soft Matter*, 2013, **9**, 7000–7006.

52 S. Asakura and F. Oosawa, *Journal of Polymer Science Part A: Polymer Chemistry*, 1958, **33**, 183–192.

53 R. F. Capellmann, N. E. Valadez-Pérez, B. Simon, S. U. Egelhaaf, M. Laurati and R. Castañeda-Priego, *Soft matter*, 2016, **12**, 9303–9313.

54 M. Kohl, R. Capellmann, M. Laurati, S. Egelhaaf and M. Schmiedeberg, *Nature communications*, 2016, **7**, 11817.

55 A. J. Liu, S. R. Nagel, W. van Saarloos and M. Wyart, *Dynamical heterogeneities in glasses, colloids, and granular media*, Oxford University Press, 2010, ch. 9.

56 A. Basu, Q. Wen, X. Mao, T. C. Lubensky, P. A. Janmey and A. G. Yodh, *Macromolecules*, 2011, **44**, 1671–1679.

57 A. Zaccone and E. Scossa-Romano, *Phys. Rev. B*, 2011, **83**, 184205.

58 A. Zaccone, J. R. Blundell and E. M. Terentjev, *Phys. Rev. B*, 2011, **84**, 174119.

59 M. Gardel, J. H. Shin, F. MacKintosh, L. Mahadevan, P. Matsudaira and D. Weitz, *Physical Review Letters*, 2004, **93**, 188102.

60 T. Gibaud, A. Zaccone, E. Del Gado, V. Trappe and P. Schurtenberger, *Phys. Rev. Lett.*, 2013, **110**, 058303.

61 S. Zhang, L. Zhang, M. Bouzid, D. Z. Rocklin, E. Del Gado and X. Mao, *Physical review letters*, 2019, **123**, 058001.

62 K. M. Smith, A. San-Miguel and L. C. Hsiao, *Physics of Fluids*, 2021, **33**, 033113.